ELSEVIER

Contents lists available at ScienceDirect

# Sensors and Actuators: B. Chemical

journal homepage: www.elsevier.com/locate/snb





# Facile synthesis of ZnO-SnO<sub>2</sub> hetero-structured nanowires for high-performance NO<sub>2</sub> sensing application

Sikai Zhao <sup>a,c,d</sup>, Yanbai Shen <sup>a,b,\*</sup>, Roya Maboudian <sup>c,d,\*</sup>, Carlo Carraro <sup>c,d</sup>, Cong Han <sup>a</sup>, Wengang Liu <sup>a</sup>, Dezhou Wei <sup>a</sup>

- <sup>a</sup> School of Resources and Civil Engineering, Northeastern University, Shenyang 110819, China
- <sup>b</sup> State Key Laboratory of Rolling and Automation, Northeastern University, Shenyang 110189, China
- <sup>c</sup> Department of Chemical and Biomolecular Engineering, University of California, Berkeley, California, 94720, USA
- <sup>d</sup> Berkeley Sensor & Actuator Center, University of California, Berkeley, California, 94720, USA

#### ARTICLE INFO

Keywords: ZnO-SnO<sub>2</sub> Heterostructure Nanowire NO<sub>2</sub> gas sensing

#### ABSTRACT

 $SnO_2$  nanoparticles were uniformly grown on the surfaces of ZnO nanowires by a simple hydrothermal process to form one-dimensional ZnO-SnO $_2$  hetero-structured nanowires. The morphology, microstructure, and composition of the pristine ZnO and ZnO-SnO $_2$  hetero-structured nanowires were characterized by X-ray diffraction, scanning and transmission electron microscopies and X-ray photoelectron spectroscopy. A systematic investigation on their gas sensing characteristics was performed using a static gas sensing measurement system. The ZnO-SnO $_2$  hetero-structured nanowires exhibited an overall enhancement in NO $_2$  sensing properties, which was found to be closely related to their Sn/Zn atomic ratio. The highest NO $_2$  response was obtained for ZnO-SnO $_2$  hetero-structured nanowires with Sn/Zn atomic ratio of 5% and at operating temperature of 150 °C. Compared with pristine ZnO nanowires, these hetero-structured nanowires also exhibited faster response/recovery rate and better NO $_2$  selectivity. The difference in sensing performance between pristine ZnO nanowires and ZnO-SnO $_2$  heterostructures are explained based on the surface depletion model and the potential barrier control model.

## 1. Introduction

Nitrogen dioxide (NO<sub>2</sub>) is a highly reactive and toxic gas that is primarily emitted from various combustion processes, such as in power plants and transportation vehicles [1]. NO<sub>2</sub> has been recognized as one of the main sources of air pollution by the World Health Organization due to its serious effect on both environment and human health [2]. It plays a major role in the formation of particulate matter  $PM_{2.5}$ , acid rain, and photochemical smog [3]. It can also cause great damage to the human respiratory system and lung even upon exposure to a trace concentration [4]. Therefore, the efficient detection and monitoring of  $NO_2$  is of great importance.

Due to their low cost, feasibility in practice, and easy integration, metal oxide semiconducting (MOS) gas sensors have drawn great attention in detecting volatile organic compounds, flammable, explosive, toxic, and harmful gases [5–7]. The ability of the MOS materials to identify the target gases is based on their resistance change upon exposure to different gaseous atmospheres. As an interfacial phenomenon, the gas sensing process typically involves two steps: (1) interaction

between the gas and the surface of sensing material; (2) transformation of the interfacial effects to measurable electrical signal (usually electrical resistance). These two parts are generally referred as the receptor function and transducer function of a gas sensor, respectively [8]. From this point of view, the accessibility of the gas molecules to the surface of the sensing material and their interaction efficiency are the primary considerations in the design of the high-performance MOS gas sensing materials

The former one depends highly on the morphology and structure of the materials. Up to date, various MOS gas sensing materials with different morphologies and structures in nano- and micro-scale have been synthesized and investigated. These materials range from zero- to three-dimensional structures, such as quantum dots, nanoparticles, nanowires, nanofilms, and various hierarchical structures [9–13]. Generally, in the structural design of the MOS gas sensing materials, a large specific surface area is considered first, which is expected to provide more adsorption and reaction sites [14]. However, the specific surface area of the sensing layer on the electrodes does not always show a positive relationship to that of the sensing materials [15]. For example,

E-mail addresses: shenyanbai@mail.neu.edu.cn (Y. Shen), maboudia@berkeley.edu (R. Maboudian).

<sup>\*</sup> Corresponding authors.

S. Zhao et al.

when nanoparticles with small size are used as the sensing units, the large specific surface area is easily restricted by their agglomeration when coating or printing on the electrodes to form the sensing layer. Thus, constructing a stable sensing layer with a large available surface area is of central importance. In addition, the interconnectivity of the sensing materials affects the gas sensing performance significantly [16]. On the one hand, the change in the potential barriers between the grains is one of the sensing mechanisms. On the other hand, sufficient effective pathways are required for electron transport through the sensing layer. However, in the present MOS gas sensors, the sensing layers are primarily in the form of thick films, while in order to ensure the entire sensing material can be involved in the gas sensing process, a porous film with sufficient gas penetration channels is needed. To address these, several structures such as porous films and three-dimensional mesoporous materials have been reported [17,18]. In particular, one-dimensional nanowires have recently received considerable attention for the applications in chemical sensing [19,20]. As ideal building blocks for gas sensing, nanowires have unique advantages of large specific surface area, high crystallinity, and high electron conduction efficiency [21]. Meanwhile, the surface of nanowires can provide a porous network, which allows the gases to diffuse and penetrate rapidly into the whole sensing film. In this way, the sensing materials can be more efficiently affected by the surrounding gaseous compositions, thereby achieving enhanced gas sensing performance [22,23].

Some strategies have been proposed to control the surface properties of pristine MOS materials and thereby improve their gas sensing characteristics. The most common method is doping or loading with noble metals, such as Au, Pt, Pd, and Ag, which are effective catalysts for gas sensing reactions [24–27]. In addition, the relationship between surface acidity/basicity and sensing properties of MOS gas sensing materials have been investigated, and some rare earth elements and their oxides have been considered as surface property regulators [28]. The crystal-facets-controlled synthesis is yet another promising way to effectively enhance the gas sensing properties [29,30]. But the materials with specific exposed facets of high surface energy and activity are usually unstable and difficult to prepare.

In recent years, many MOS composites are shown to exhibit better gas sensing properties than the single ones, resulting in increased interests in MOS-MOS heterostructures, which are cost-effective, stable, and easy to synthesize [31–33]. Although various strategies are being explored to achieve better sensing performance to different target gases, the classification of the host sensing materials is always the most crucial factor. Based on the previous reports,  $\mathrm{SnO}_2$  and  $\mathrm{ZnO}$  stand out from various other materials and have been recognized as the most promising sensing materials for high-performance MOS gas sensors [34].

In this paper, a high-performance gas sensing material is designed and demonstrated. Firstly, ZnO nanowires are prepared via a simple hydrothermal process. Then,  $SnO_2$  nanoparticles with 3–5 nm in diameters are grown on their surface to construct ZnO-SnO $_2$  n-n heterostructures. The morphology, microstructure, and gas sensing performance of pristine ZnO and ZnO-SnO $_2$  heterostructures are studied. Based on these, possible sensing enhancement mechanisms of ZnO-SnO $_2$  heterostructures are discussed.

# 2. Experimental

# 2.1. Chemicals

Zinc acetate dihydrate  $(Zn(CH_3COO)_2\cdot 2H_2O)$ , polyethylene-400 (PEG-400), absolute ethanol  $(C_2H_5OH)$ , sodium hydroxide (NaOH), stannous chloride dehydrate  $(SnCl_2\cdot 2H_2O)$ , and trisodium citrate dehydrate  $(Na_3C_6H_5O_7\cdot 2H_2O)$  were purchased from Sinopharm Chemical Reagent Co., Ltd. Sodium dodecyl sulfate (SDS) was purchased from Shanghai Macklin Biochemical Co., Ltd. All the chemicals were analytical grade and used as purchased without further purification.

#### 2.2. Synthesis of ZnO nanowires

ZnO nanowires were synthesized via a simple solvothermal method. In a typical procedure, 0.44 g Zn(CH $_3$ COO) $_2\cdot 2H_2$ O, 0.1 g SDS, 27 mL PEG400, and 117 mL ethanol were added into a beaker and magnetically stirred for 1 h at room temperature to form homogeneously solution. Then the obtained solution was poured into a 200 mL Teflon-lined stainless-steel autoclave. The reaction process was conducted by setting the autoclave in an electric oven at 140  $^{\circ}$ C for 16 h, followed by natural cool down to room temperature. The resulting white products were collected and cleaned with ethanol and distilled water to remove the impurities. Finally, the samples were dried at 60  $^{\circ}$ C for several hours in a vacuum drying chamber.

# 2.3. Synthesis of ZnO-SnO2 hetero-structured nanowires

ZnO-SnO $_2$  hetero-structured nanowires were prepared as follows. 0.678 g SnCl $_2$ ·2H $_2$ O and 1.323 g Na $_3$ C $_6$ H $_5$ O $_7$ ·2H $_2$ O were dissolved in 30 mL distilled water, referred to as solution (A). Various volumes of solution (A) were added into 40 mL deionized water and magnetically stirred for 10 min to form solution (B). Then 0.0972 g of as-prepared ZnO nanowires were evenly dispersed in solution (B) by ultrasonication and magnetically stirring. The obtained suspensions were transferred into a 200 mL Teflon-lined stainless-steel autoclave and heated at 120 °C for 6 h. After that, the derived products were centrifuged and washed with deionized water and ethanol, dried at 60 °C for several hours, and annealed at 500 °C for 3 h.

#### 2.4. Characterizations

The structures of the prepared samples were investigated using X-ray diffraction (XRD) (PANalytical X'Pert Pro, Cu K $\alpha$  radiation,  $\lambda=1.5406$  Å) operating at a generator voltage and current of 40 kV and 40 mA, respectively. The morphology and structure of the products were studied by scanning electron microscopy (SEM, Hitachi S-4800) working at 2 kV. Transmission electron microscopy (TEM) images, high-resolution transmission electron microscopy (HRTEM) pattern, fast Fourier transform (FFT) spectra, and energy-dispersive X-ray spectroscopy (EDS) elemental maps were recorded by JEM-2100 F microscope with accelerating voltage of 200 kV. X-ray photoelectron spectroscopy (XPS) analysis was carried out using a Thermo Scientific Escalab 250Xi with the K $_{\alpha}$  source of monochromatic Al.

# 2.5. Fabrication and measurement of gas sensors

The detailed structure and fabrication process of the gas sensing devices have been presented in our previous reports [35,36]. Briefly, on each end of a ceramic tube (internal diameter =0.8 mm, external diameter =1.2 mm, length =4 mm), a 0.5 mm-wide gold films were printed as the electrodes. A pair of Pt wires were then welded to each Au electrode. The as-prepared samples were uniformly dispersed in a proper amount of ethanol, and subsequently coated on the outer surface of the ceramic tube. The operating temperature of the sensor device was controlled by adjusting the voltage across a Ni-Cr alloy wire that was inserted inside the ceramic tube. Before testing, the sensor was heated at 325  $^{\circ}\mathrm{C}$  and maintained for 48 h to improve its stability.

Gas sensing measurements were conducted on a WS-30A commercial testing system (Winsen Electronics Science and Technology Co., Ltd., Henan Province, China), which was reported previously [37]. During testing, a predefined volume of  $NO_2$  (0.05 %, Dalian special gases, CO., LTD) was injected into the 18 L test chamber from the gas injection inlet using a syringe and then mixed with air by a mini-fan. When the sensor response reached a stable value,  $R_g$ , the cover of the test chamber was removed to exhaust the  $NO_2$  and expose the sensor to the air,  $R_a$ , again in a fume hood. The sensing data were recorded once per second during the whole sensing process. The relative humidity (RH) during the sensing

tests was maintained around 25 %. The sensor response (S) to the target gas is defined as  $S=R_a/R_g$  and  $S=R_g/R_a$  for reducing and oxidizing gases, respectively. The response and recovery times of the sensor are defined as the times required to reach 90 % resistance variation when the analyte gas is injected and exhausted, respectively. To assess the selectivity of the sensor, hydrogen (10 % in N<sub>2</sub>, Dalian special gases, CO., LTD) were introduced to the gas chamber following a similar process as described above for NO<sub>2</sub>. Acetone, methylbenzene, ammonia, and formaldehyde gas were obtained by evaporating the corresponding liquids while the sulfur dioxide gas was obtained by evaporating sulfurous acid. All the used liquid reagents for testing were analytical grade and purchased from Sinopharm Chemical Reagent Co., Ltd.

#### 3. Results and discussion

#### 3.1. Characterizations

Fig. 1 shows representative XRD spectra obtained on the pristine ZnO nanowires and ZnO-SnO2 heterostructures corresponding to Sn/Zn atomic ratios of 1%, 5%, and 30 % (referred to as Sn/Zn1, Sn/Zn5, and Sn/Zn30, respectively). For pristine ZnO nanowires, all the observed diffraction peaks in Fig. 1(a) are well indexed to wurtzite structured ZnO (ICCD file No. 79-0206). However, there are no visible Sn-related peaks in the XRD patterns of the samples Sn/Zn1 (Fig. 1(b)) and Sn/Zn5 (Fig. 1 (c)), although the Sn element was introduced during the second hydrothermal reaction process and SnO2 nanoparticles can be clearly observed on the surface of ZnO nanowires by SEM and TEM characterizations (Figs. 2 and 3). This could be attributed to the low atomic ratio of Sn/Zn and the ultra-fine physical size of SnO<sub>2</sub> nanoparticles (Fig. 3). As the Sn/Zn atomic ratio increases to 30 %, the emerged new peaks in Fig. 1(d) can be ascribed to the tetragonal SnO<sub>2</sub> (ICCD file No. 88-0287). In addition, the absence of the diffraction peaks to any impurities indicates the prepared samples are of high phase purity.

Fig. 2 displays representative SEM images of the prepared samples at different magnifications. As can be seen in Figs. 2(a,b), the pristine ZnO nanowires show a smooth surface and large length-to-diameter ratios, with lengths in 500 nm to several micrometers range and diameters in 30–50 nm range. When the Sn element is introduced by using the hydrothermal reaction process, SnO<sub>2</sub> nanoparticles with a diameter of 3–5 nm can be clearly observed on the surface of ZnO nanowires (Figs. 2(d,f, h)). Meanwhile, as designed and expected, SnO<sub>2</sub> nanoparticles are homogeneously formed on the surface of the pre-synthesized ZnO nanowires, and the density of surface-loaded SnO<sub>2</sub> nanoparticles gradually grows with the increase of Sn content in the precursor solution.

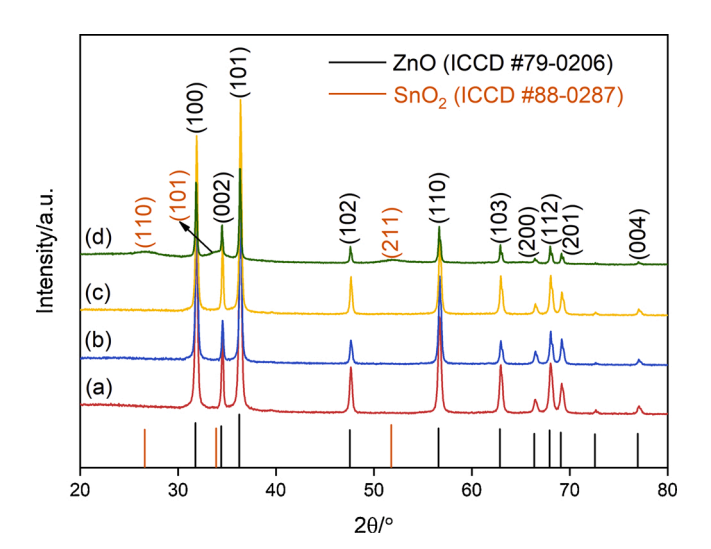


**Fig. 1.** XRD patterns of the as-synthesized samples. (a) Pristine ZnO nanowires; (b) Sn/Zn1; (c) Sn/Zn5; (d) Sn/Zn30.

Furthermore, the aggregation of  $SnO_2$  nanoparticles can be clearly observed when the Sn/Zn atomic ratio increases to 30 %.

The detailed structural analyses of ZnO-SnO2 hetero-structured nanowires were carried out by TEM. Fig. 3 shows representative results obtained on the Sn/Zn5 sample. From the low-magnification TEM images in Figs. 3(a, b), the wire-shaped nanostructure with a rough surface can be clearly observed, the diameter of which is uniformly 30–50 nm throughout the length, consistent with the SEM results. The high-magnification TEM image in Fig. 3(c) indicates that the assynthesized one-dimensional structure is comprised of nanowire decorated with spherical nanoparticles. Specifically, the nanoparticles are 3–5 nm in diameter and uniformly distributed on the nanowires surface, forming the heterostructure. The EDS spectrum in Fig. 3(d) confirms the presence of Zn, O, and Sn elements in the composites. The calculated Sn/ Zn atomic ratio is about 4.9 % which matches that in the precursor solution, indicating that almost all Sn<sup>2+</sup> ions in the precursor solution is converted into SnO2. Figs. 3(e,f) present the HRTEM image and the corresponding FFT spectra, respectively. In agreement with the XRD results, the clear lattice interplanar distance value of 2.5 Å can be theoretically assigned to the (101) crystal planes of wurtzite structured ZnO, while 3.3 Å matches well with the (110) crystal planes of tetragonal structured SnO<sub>2</sub>. Figs. 3(g-j) display the elemental mapping images of a single ZnO-SnO<sub>2</sub> hetero-structured nanowire. It can be seen that the elements Sn, Zn, and O are distributed uniformly along the nanowire, demonstrating that SnO2 nanoparticles are evenly grown on the surface of ZnO nanowires without local agglomeration. Furthermore, the significantly lower density of Sn element than Zn and O elements is in good agreement with the relative amount of Sn, Zn, and O elements in the precursor solution.

X-ray photoelectron spectroscopy was carried out on the samples to investigate their surface compositions. Fig. 4 shows representative XPS results obtained on the Sn/Zn5 sample. All the peaks were calibrated by using C 1s peak at 284.8 eV as the reference. The full scan spectrum in Fig. 4(a) confirms the as-prepared Sn/Zn5 is composed of Zn, O, and Sn elements with high purity. Fig. 4(b) shows the close-up scan of the Zn 2p region, in which the peak located at the binding energy of 1021.67 eV can be indexed to Zn 2p<sub>3/2</sub>, while the peak located at the binding energy of 1044.70 eV is attributed to Zn  $2p_{1/2}$  [38]. Fig. 4(c) gives the close-up scan of Sn 3d region in the binding energy range of 480-500 eV. Three peaks centered at 486.77, 495.12, and 498.16 eV can be clearly observed. According to the standard XPS spectrum of the oxidized Sn, the spin-orbit splitting value of Sn 3d is around 8.4 eV [39]. Thus the peaks around 486.77 and 495.12 eV can be assigned to Sn 3d<sub>5/2</sub> and Sn 3d<sub>3/2</sub>, respectively, pertaining to Sn<sup>4+</sup> cations [40]. Furthermore, the peak located at 498.16 eV is attributed to Zn LM2 Auger line [41]. The chemical state of oxygen in the ZnO-SnO2 hetero-structured nanowires was also investigated. As shown in Fig. 4(d), the broad and asymmetric curve is deconvoluted into two peaks, demonstrating the different chemical environments of oxygen. The peak centered at the lower binding energy of 530.39 eV is typically ascribed to the lattice O<sup>2-</sup> in SnO<sub>2</sub> and ZnO, while the peak located at the higher binding energy of 531.37 eV is assigned to the surface adsorbed oxygen species (e.g. physisorbed, chemisorbed, dissociated, and hydroxyl related oxygen species), the content and activity of which have a significant effect on the gas sensing characteristics of the sensing materials [36,42-44].

# 3.2. Gas sensing properties

As shown in many reports, the sensing characteristics of the MOS sensors highly depend on their operating temperature due to the strong relationship between temperature and the gas adsorption-desorption processes on the surface of the sensing materials [45]. Therefore, the gas sensing properties of the as-prepared sensors under different operating temperatures were compared first. Fig. 5 shows the responses, S, of the four sensors towards 1 ppm  $NO_2$  as a function of the operating temperature. For all sensors, the response increases with increasing

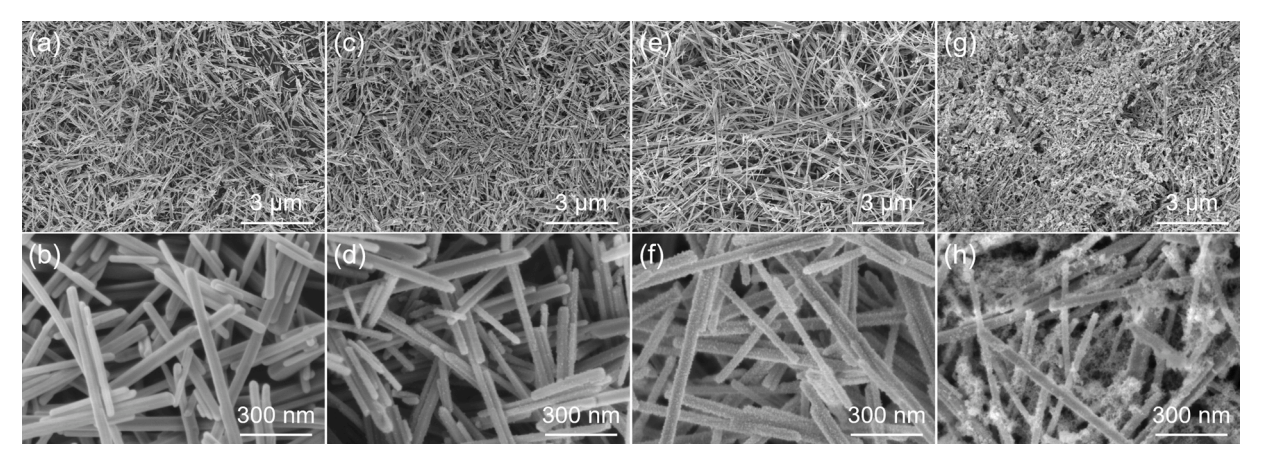


Fig. 2. Low-magnification and high-magnification SEM images of the as-synthesized samples. (a, b) Pristine ZnO nanowires; (c, d) Sn/Zn1; (e, f) Sn/Zn5; (g, h) Sn/Zn30.

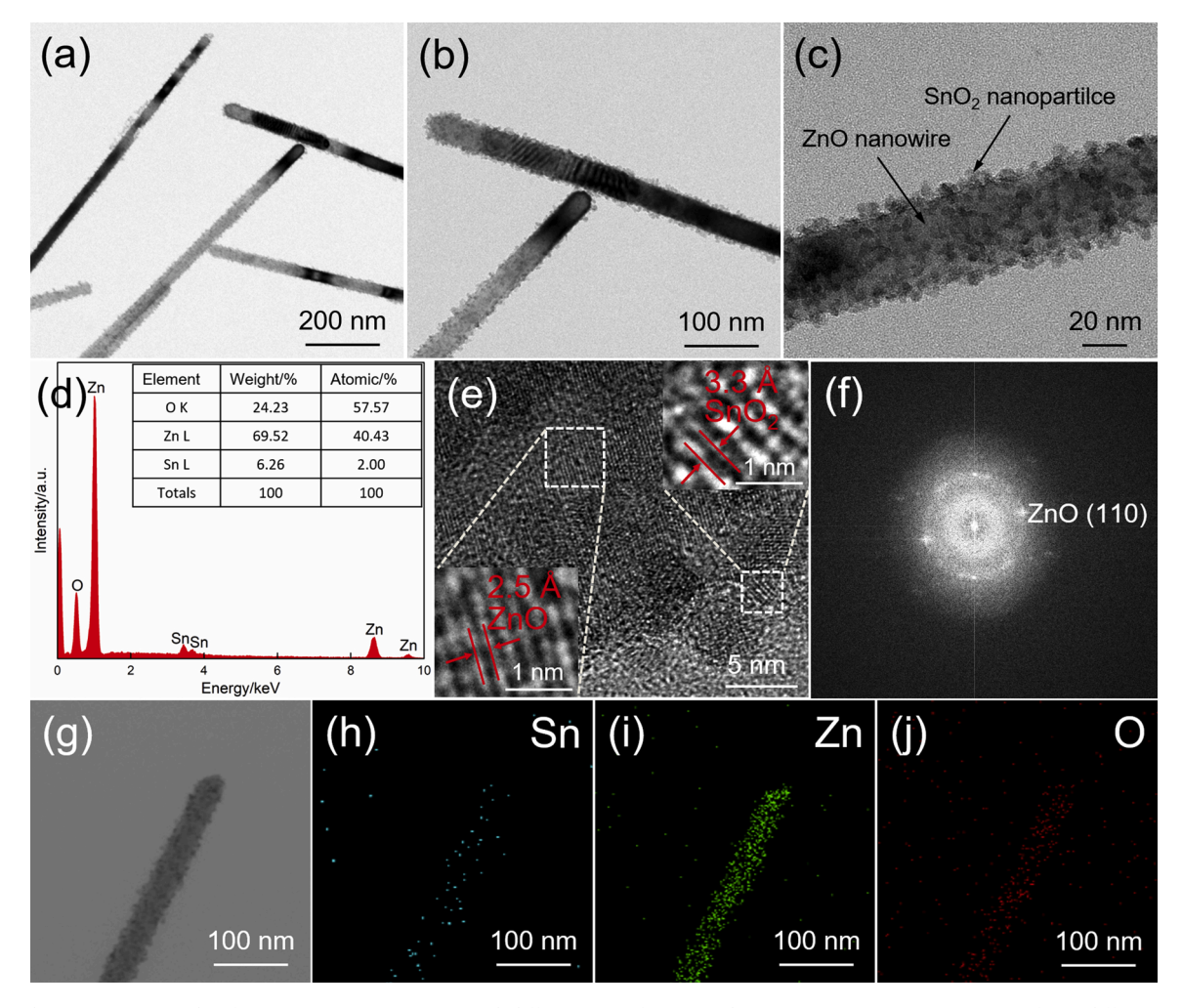


Fig. 3. TEM characterization results of Sn/Zn5. (a~c) TEM images with different magnifications; (d) EDS spectrum; (e) HRTEM image; (f) FFT diffractogram; (g~j) A single nanowire of Sn/Zn5 and its elemental mapping images.

operating temperature reaching the highest value at 150  $^{\circ}$ C, then decreases with further increase in the operating temperature. The observed behavior can be explained as follows. For MOS resistive gas sensors, the change in the resistance of the sensing material is determined by dynamic interactions between the gas molecules and the sensing material surfaces. At low temperatures, the NO<sub>2</sub> molecules do not have enough activation energy to adsorb on the surfaces of the sensing materials or to

react with the surface chemisorbed oxygen species, resulting in a low sensor response [46]. On the other hand, at high operating temperature,  $NO_2$  molecules tend to desorb from the sensing materials instead of adsorbing on it; in addition, the oxygen species chemisorbed on the sensing materials can desorb before reacting with  $NO_2$ . Consequently, a peak in sensor response is observed as a function of operating temperature, corresponding to a balance between the opposing processes.

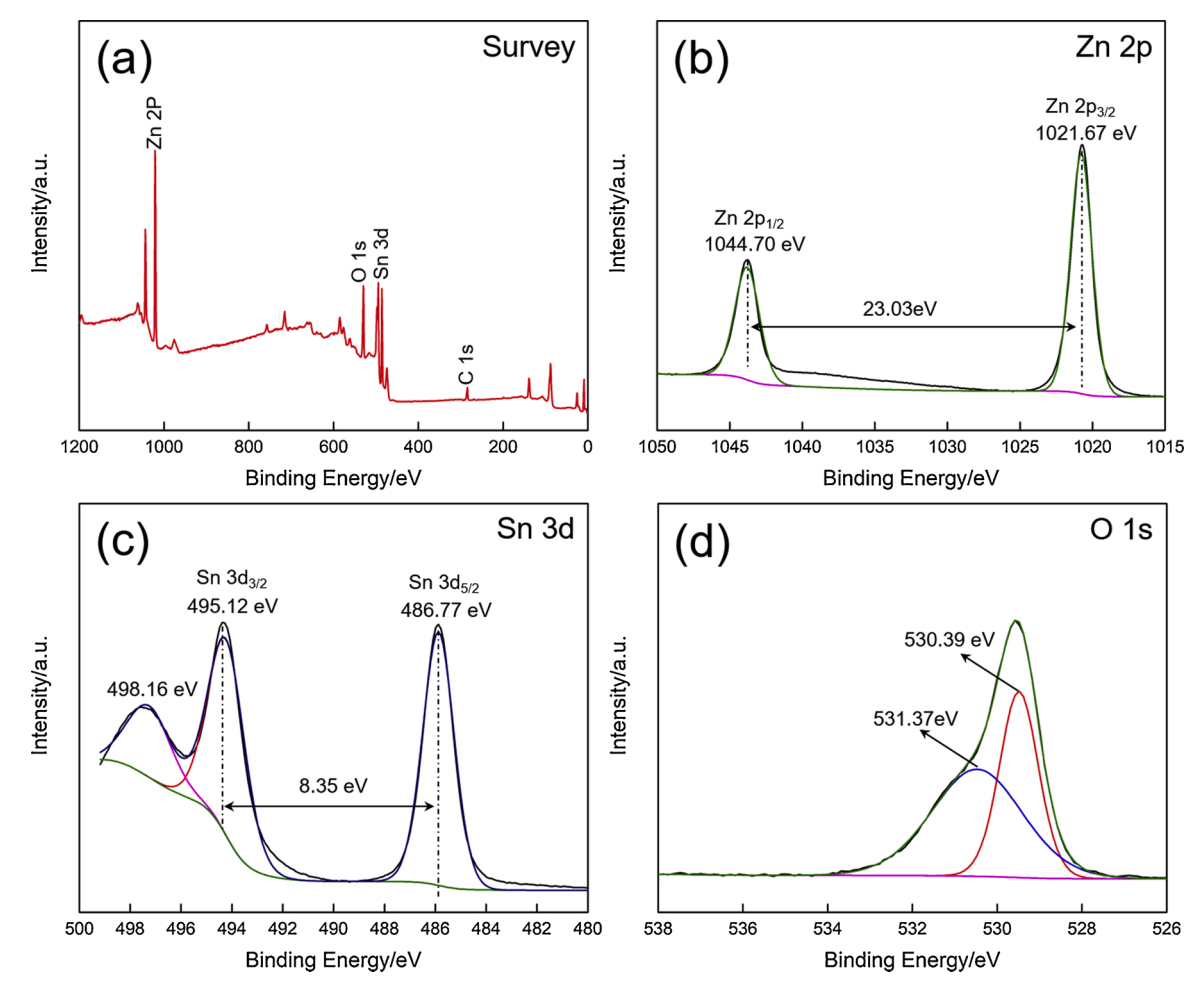


Fig. 4. XPS analysis results of Sn/Zn5. (a) Survey spectrum; (b) Zn 2p spectrum; (c) Sn 3d spectrum; (d) O 1s spectrum.

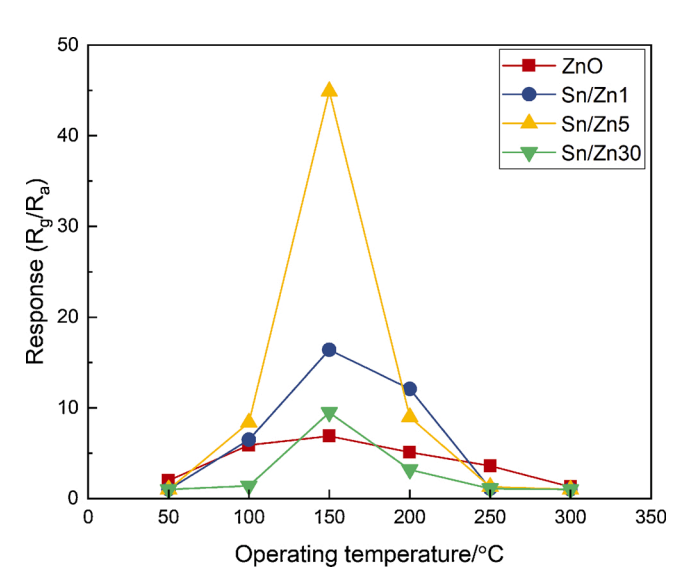


Fig. 5. Responses of the sensors upon exposure to 1 ppm  $\mathrm{NO}_2$  at different operating temperatures.

As depicted in Fig. 5, the optimum operating temperature of pristine ZnO nanowires for  $NO_2$  detection is not affected by the surface-loading of  $SnO_2$  nanoparticles. This behavior suggests that the host ZnO nanowires still play the main role in the gas sensing process after the formation of the n-n junction, as also found in some recent reports [47,48].

However, Fig. 5 also shows that  $ZnO-SnO_2$  nanocomposites exhibit a significant enhancement in  $NO_2$  response over the pristine ZnO nanowires, and the maximum response of about 45 is obtained for the sensor Sn/Zn5, which is 6.5 times higher than the response on pristine ZnO nanowires. Thus, it can be concluded that a proper amount of surface loading of  $SnO_2$  nanoparticles is a promising method to improve the response of pristine ZnO nanowires to  $NO_2$ .

Fig. 6 shows the transient response of the sensors as a function of NO<sub>2</sub> concentration. Also, the dynamic response and recovery curves of the sensors at different operating temperatures can be seen Figure S1. For all sensors, the resistances increase to reach a stable value when NO2 is introduced, and then completely recover to their initial state after exhausting NO2 and being surrounded by fresh air again. On the one hand, the results indicate the excellent reversibility of the sensors to NO<sub>2</sub>; on the other hand, the results demonstrate the n-type semiconducting conduction characteristics of the as-synthesized pristine ZnO and ZnO-SnO<sub>2</sub> heterostructures. An enhanced response can be clearly observed towards a higher NO2 concentration. In particular, the response of the Sn/Zn5 sensor exhibits a more noticeable increase with increasing NO<sub>2</sub> concentration over the other three sensors. Furthermore, the response transition behaviors of "sharp increase-stable-return to initial" in each "air-NO2-air" sensing cycle confirm the excellent reversibility and reproducibility of the sensors. Moreover, the limit of detection of the sensors are estimated to be 30, 1542, 2.5, and 35 ppb for ZnO, Sn/Zn1, Sn/Zn5, and Sn/Zn30, respectively, corresponding to signal-to-noise ratio of 3 [49,50] (See the supplementary information).

Based on the results in Fig. 6, the sensor response as well as the response/recovery times of the four sensors are calculated and

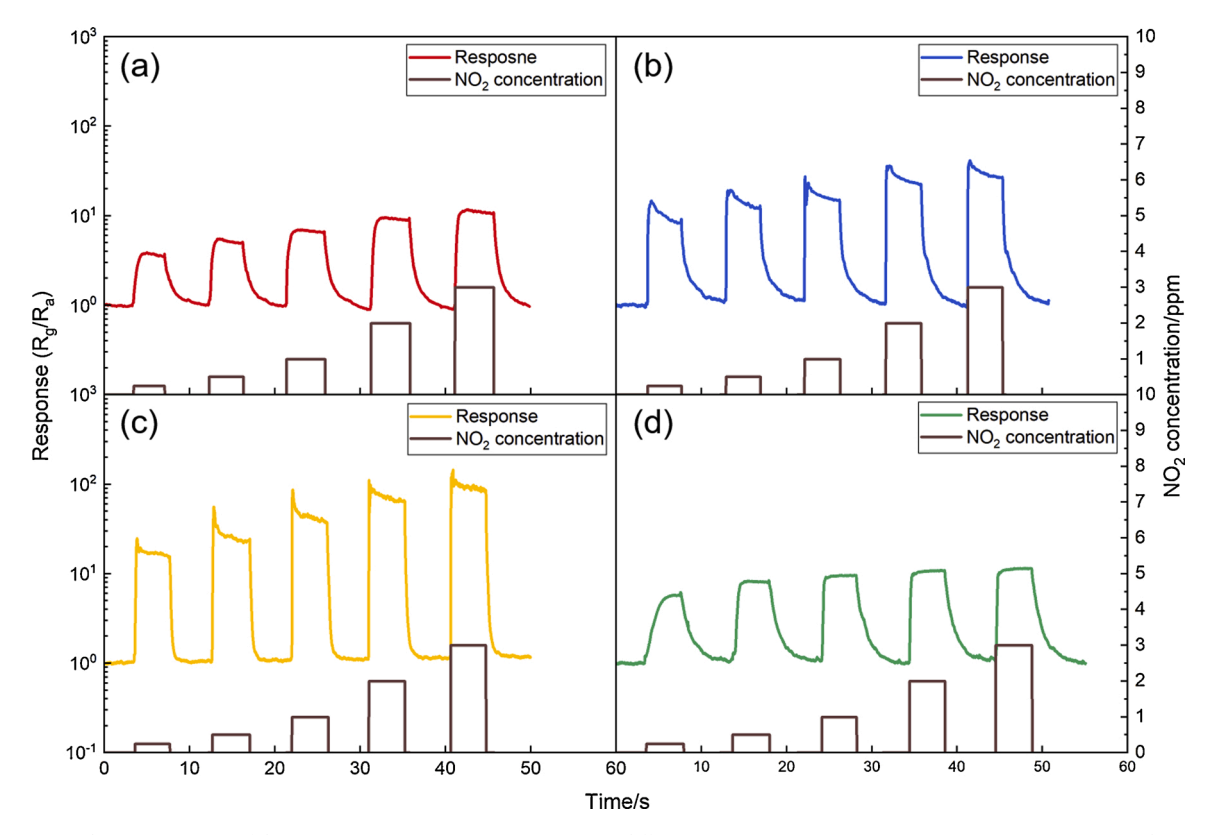


Fig. 6. Response and recovery curves of the sensors upon exposure to 1 ppm  $NO_2$  at different operating temperatures. (a) Pristine ZnO nanowires; (b) Sn/Zn1; (c) Sn/Zn5; (d) Sn/Zn30.

illustrated in Fig. 7. As presented in Fig. 7(a), the response of all sensors increases monotonically with increased NO $_2$  concentration. The data show that the Sn/Zn5 sensor exhibits the highest response to each NO $_2$  concentration ranging from 250 ppb to 3 ppm. To better compare the gas sensing performance of the four sensors, the sensor responses to 1 ppm NO $_2$  at 150 °C are given in Fig. 7(a) inset. It can be observed that the response is significantly improved by the surface-loaded SnO $_2$  nanoparticles, increasing rapidly with increasing SnO $_2$  content. The response then falls by further increasing the Sn/Zn atomic ratio above 5%. As can be seen in the SEM characterization results (Fig. 2), for Sn/Zn30, the SnO $_2$  nanoparticles show serious agglomeration and the surfaces of ZnO nanowires are almost fully covered by these aggregated SnO $_2$  nanoparticles. Considering that the host ZnO nanowires may still play a

critical role in the gas sensing process for the  $ZnO-SnO_2$  composites, the decreased response at  $150\,^{\circ}C$  may be mainly ascribed to the aggregation of  $SnO_2$  nanoparticles and the decrease of the active sites on the surfaces of ZnO nanowires [51,52]. Therefore, to achieve a high  $NO_2$  response, the content of the surface-loaded  $SnO_2$  must be controlled.

Fig. 7(b) gives the response and recovery times of the sensors towards 1 ppm NO<sub>2</sub> at 150 °C. For all four sensors, the response time is shorter than the recovery time, which is also observed for many other MOS gas sensing materials reported previously [53–55]. A possible explanation was proposed by Song et al. [56,57], where they pointed out that response time ( $t_{\rm res}$ ) and recovery time ( $t_{\rm rec}$ ) may be related to the forward ( $\Delta E_{\rm res}$ ) and reverse ( $\Delta E_{\rm rec}$ ) reaction barrier heights, respectively. Following the same analysis (detailed in the supplementary

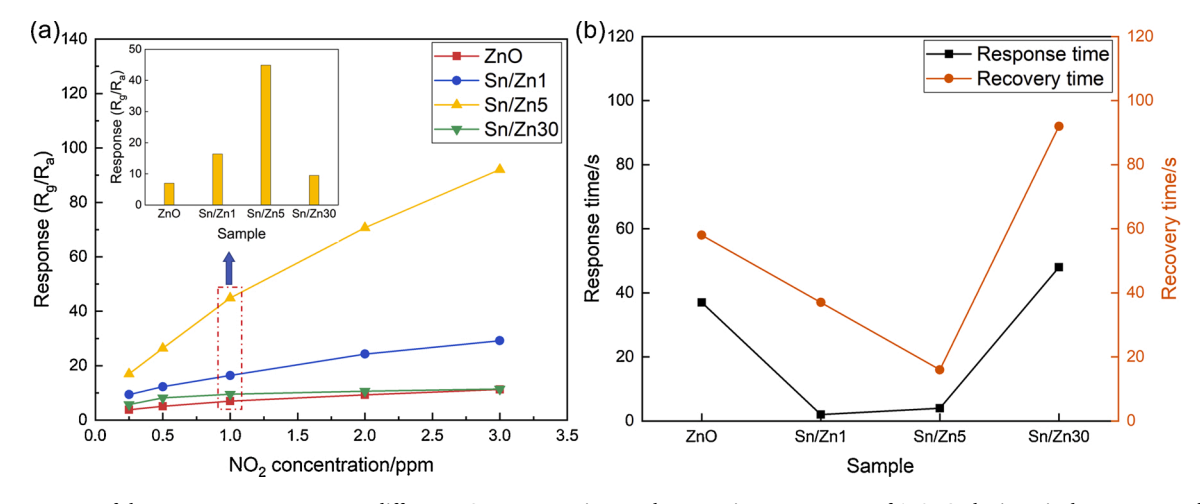


Fig. 7. (a) Responses of the sensors upon exposure to different NO<sub>2</sub> concentrations at the operating temperature of 150 °C, the inset is the responses of the sensors upon exposure to 1 ppm NO<sub>2</sub> at 150 °C; (b) Response and recovery times of the sensors upon exposure to 1 ppm NO<sub>2</sub> at the operating temperature of 150 °C.

information), the calculated  $\Delta E_{\rm res}$  and  $\Delta E_{\rm rec}$  values in present study are 288 and 333 meV for pristine ZnO, and 266 and 393 meV for Sn/Zn5. It can be found that, for both pristine ZnO and Sn/Zn5, the reverse reaction barrier heights are higher than the forward reaction barrier heights which would result in their longer recovery times than response times. Furthermore, the response and recovery times of the sensor Sn/Zn5 were 4 s and 16 s, respectively, at 150 °C. Such short response/recovery times suggest that the ZnO-SnO2 composites have a promising application prospect in real-time NO2 monitoring.

To investigate the repeatably and stability of the sensors, several successive sensing cycles were applied to the sensors. Fig. 8 shows representative behavior in response to 1 ppm  $NO_2$ . As can be seen in this figure, similar dynamic response and recovery characteristics are seen for all sensors after each cycle. Furthermore, no shift of the baseline resistance is observed after each sensing cycle. All the above observations give strong evidence for the excellent reproducibility and cyclic stability of the present sensors.

The specific recognition of the target gas is one of the most essential and fundamental abilities of a high-performance gas sensor. Fig. 9 shows the responses of the pristine ZnO nanowires and Sn/Zn5 sensors to NO<sub>2</sub> and various interference gases (including acetone, methylbenzene, ammonia, formaldehyde, sulfur dioxide, methane, and hydrogen) at the operating temperature of 150 °C. The pristine ZnO nanowires show a higher response to 1 ppm NO2 than to other interference gases with much higher concentration, indicating its good NO2 identification ability. However, after constructing the heterostructure by surface loading of SnO2 nanoparticles, the response of the ZnO nanowires to NO2 is remarkably improved, while a slight or no obvious enhancement in response to the interference gases is observed. Thus, the NO2 selectivity of the ZnO nanowires is significantly improved by the addition of SnO2 nanoparticles. Three reason should be responsible for the much higher NO2 response of Sn/Zn5 over other gases. The first one is the intrinsic properties of ZnO nanowires, which play the important role in

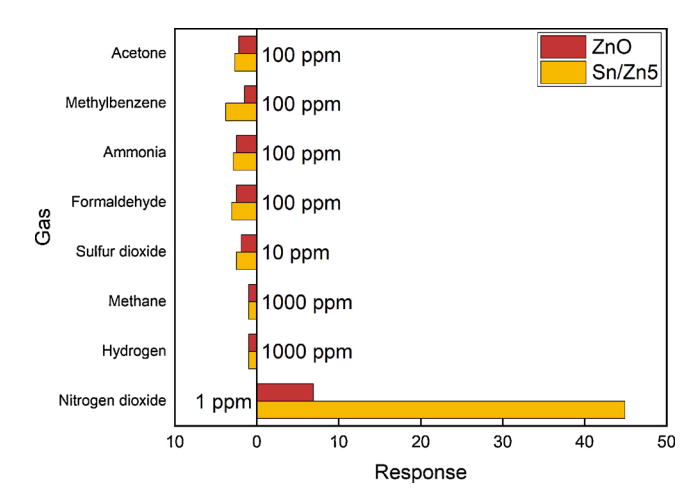


Fig. 9. Selectivity of the Pristine ZnO nanowires and Sn/Zn5 at the operating temperature of 150  $^{\circ}\text{C}.$ 

gas sensing process. The second reason may be due to the more active chemical property of  $NO_2$  than the other gases. The third one is the operating temperature. For the  $ZnO-SnO_2$  composites prepared in this study, the optimum operating temperature for  $NO_2$  sensing is determined to be  $150~^{\circ}C$ . At this temperature, the sensor shows higher response to  $NO_2$  than the other gases, while the sensor may more sensitive to other gases besides the operating temperature of  $150~^{\circ}C$ . Figure S5 gives the responses of ZnO and Sn/Zn5 to 1~ppm  $NO_2$  and 100~ppm ethanol at different operating temperatures. It can be observed that both ZnO and Sn/Zn5 show much higher response to  $NO_2$  than ethanol at  $150~^{\circ}C$ . When the operating temperature increases to  $300~^{\circ}C$ , ZnO and Sn/Zn5 exhibit negligible responses to  $NO_2$  but obvious responses to ethanol. Considering the highly close relationship between gas sensing

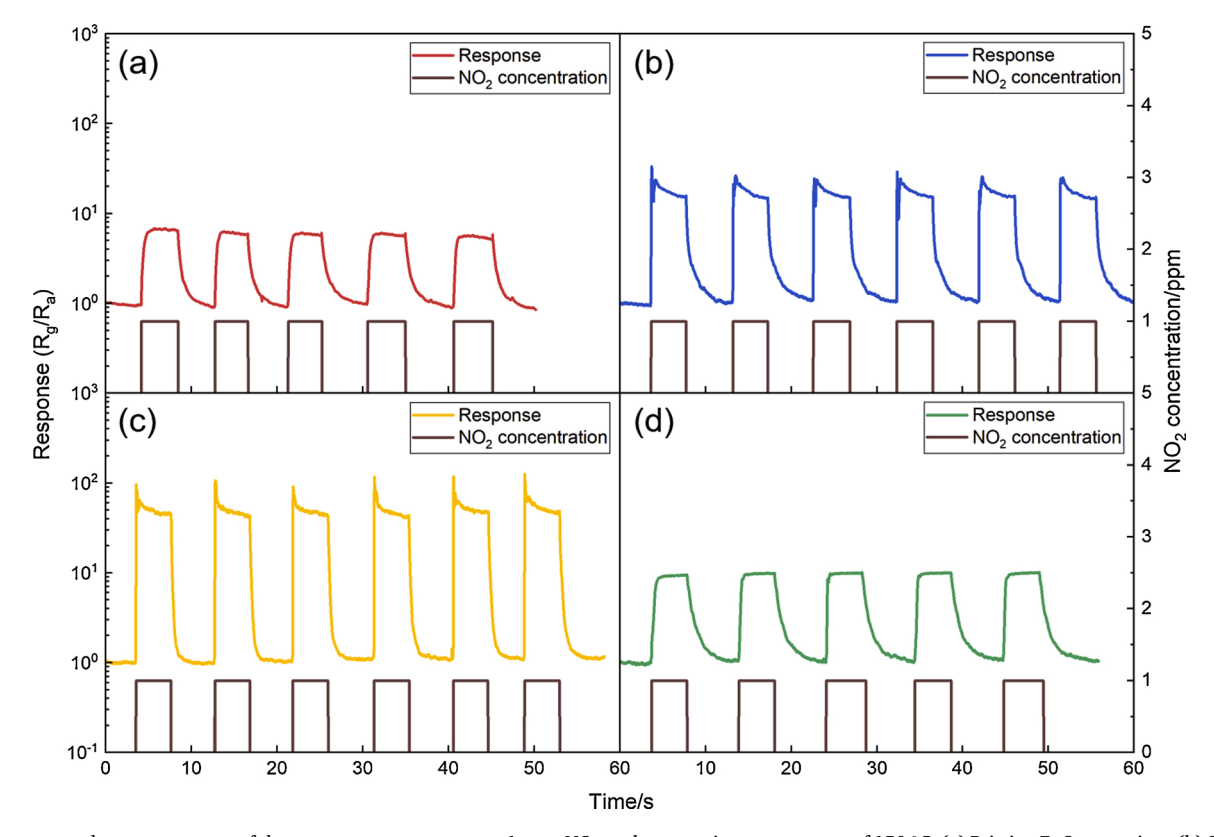


Fig. 8. Response and recovery curves of the sensors upon exposure to 1 ppm NO<sub>2</sub> at the operating temperature of 150 °C. (a) Pristine ZnO nanowires; (b) Sn/Zn1; (c) Sn/Zn5; (d) Sn/Zn30.

performance and the operating temperature, the optimal operating temperature is always firstly determined before the other gas sensing properties evaluations. The excellent selectivity of the sensor Sn/Zn5 makes it a more promising candidate than the pristine ZnO nanowire to fabricate  $NO_2$  sensing devices. Furthermore, Table 1 gives a comparison of the  $NO_2$  sensing properties of various recently reported materials, it can be seen that ZnO-SnO $_2$  hetero-structured nanowires prepared in this study show a better overall  $NO_2$  sensing performance in terms of optimum operating temperature, response, response/recovery times.

# 3.3. Sensing mechanism discussion

From the above investigations, the sensing performance of the pristine ZnO nanowires to NO2 can be comprehensively improved by constructing ZnO-SnO<sub>2</sub> heterostructure. To better understand this behavior, the NO<sub>2</sub> sensing mechanism for pristine ZnO and SnO<sub>2</sub> is first discussed. As n-type semiconductors, the sensing mechanism of pristine ZnO and SnO2 can be explained by the widely acknowledged depletion model [68]. Briefly, when the sensors are exposed to air, the oxygen molecules chemisorb on the surface of the sensing materials in the form of O<sub>2</sub>-, O-, and O<sup>2-</sup>. As a result of the electron transfer from the conduction band to the chemisorbed oxygen ions, a depletion region is formed near the surface of the sensing materials. Upon exposure to the target gases, a redox reaction occurs between the target gases and chemisorbed oxygen species, which either releases the electrons to the conduction band or further captures the electrons from the conduction band of the sensing materials, leading to the change of the surface depletion layer, and hence the sensor resistance. Generally, the reaction route for NO2 sensing process are proposed as follows [69,70]:

$$NO_2 + e \rightarrow NO_2 - \tag{1}$$

$$NO_{2-} + O_{-} + 2e_{-} \rightarrow NO + O^{2-}$$
 (2)

 $NO_2$  molecules interact with the surface of the sensing materials to form nitrogen oxide ions (Eq. (1)), which were then react with surface adsorbed oxygen (Eq. (2)). Both reactions further trap electrons from the conduction band of the sensing materials and broaden the depletion layer, which gives rise to the increase of the sensor resistance.

For the noble metal-functionalized MOS gas sensing materials, the catalytic and spillover effects of the noble metals are usually considered to be responsible for the enhanced gas sensing performance. However, the sensing mechanism of the MOS-MOS heterostructures has not been well established yet. As pointed in some recent literatures [71–74], the sensor response of MOS gas sensors can be improved by regulating the baseline resistance of the gas sensing materials. Based on these literatures, the sensors with a lower baseline resistance should show a higher (lower) response if the sensor response is defined as  $R_g/R_a$  ( $R_a/R_g$ ). In this study, although and the sensor response is defined as  $R_g/R_a$  for NO<sub>2</sub>

and the  $ZnO-SnO_2$  composites exhibit an overall higher resistance than that of pristine ZnO nanowires (Figure S1), the results show that the  $NO_2$  response of pristine ZnO nanowires can be effectively improved by  $SnO_2$ -loading. This suggests that the baseline resistance regulation is not the main factor for the mechanism of  $NO_2$  response enhancement. Based on the sensing model of pristine n-type MOS sensors described above, several possible reasons may be put forth for the enhanced  $NO_2$  sensing performance of the  $ZnO-SnO_2$  heterostructures.

First of all, the formation of the n-n junctions at the interfaces between SnO2 nanoparticles and ZnO nanowires may act as a vital part in modulating the sensing characteristics. For a better understanding, Fig. 10(a,b) give a possible energy band structure for the ZnO-SnO<sub>2</sub> heterostructure. From the previous reports [32,75], the electron affinity  $(\chi)$ , work function  $(\varphi)$ , and band gap  $(E_g)$  of SnO<sub>2</sub> are around 4.5, 4.9, and 3.5 eV, respectively, while those for ZnO are about 4.3, 5.2, and 3.37 eV, respectively. When SnO<sub>2</sub> and ZnO are brought into close contact, the electrons diffuse from SnO2 to ZnO due to the electron concentration gradient between these two materials and the higher work function of ZnO compared with SnO<sub>2</sub>. Simultaneously, a built-in electric field is formed at their interfaces, leading to an electron drift motion from ZnO to SnO<sub>2</sub>. A dynamic equilibrium of these two opposite motions is established when the Fermi levels of SnO2 and ZnO become equal. On account of the electron migration processes, an electron accumulation layer and depletion layer are formed on ZnO and SnO2 sides, respectively, resulting in an increased number of free electrons on the surface of ZnO nanowires. On the one hand, the increased free electrons are beneficial to the NO<sub>2</sub> sensing reaction route shown in Eq. 1, which can contribute to the enhanced NO2 response. Furthermore, the increased available electrons lead to an increased surface chemisorbed oxygen, namely, more oxygen species are available for the reaction process shown in Eq. 2, resulting a higher NO<sub>2</sub> response.

Second, the modulation of the potential barrier height may also be responsible for the NO2 response enhancement. As observed in SEM and TEM characterizations (Figs. 2 and 3), for the Sn/Zn5 sensor which shows the highest NO2 response, a large fraction of the surface of the host ZnO nanowires is covered by SnO2 nanoparticles. Therefore, most of the NO2 molecules interact with SnO2 nanoparticles rather than ZnO nanowires during the sensing process. Meanwhile, the diameters of these SnO<sub>2</sub> nanoparticles are characterized to be 3-5 nm, which are smaller than the reported Debye length (D<sub>I</sub>) of SnO<sub>2</sub> (18 nm ca.) [76]. Thus, SnO<sub>2</sub> nanoparticles are expected to be fully depleted in air. Accordingly, when the sensor based on the Sn/Zn5 sample is exposed to NO<sub>2</sub>, it may be hard for the NO<sub>2</sub> molecules to have a redox reaction on the surface of SnO2 nanoparticles due to the lack of the available electrons. From this perspective, if only the surface depletion model is employed to explain the sensing mechanism, the resistance change of the Sn/Zn5 sample should be smaller than the pristine ZnO nanowires, which is the opposite of the experimental results. There are similar

**Table 1**Comparison of NO<sub>2</sub> sensing properties of different sensing materials.

Materials	Operating temperature (°C)	$NO_2$ concentration (ppm)	Response	Response time (s)	Recovery time (s)	Ref.
In <sub>2</sub> O <sub>3</sub> nanosheets	250	50	164	5	14	[58]
Au/MASnI <sub>3</sub> /SnO <sub>2</sub> (MA: methylammonium cation)	Room temperature (UV light is needed)	5	240	-	12	[59]
WO <sub>3</sub> microspheres	100	5	107	>20	>90	[60]
WS <sub>2</sub> /graphene	Room temperature	1	1.2	_	_	[61]
3D graphene nanosheets	Room temperature	5	2.5	_	_	[62]
3D WO <sub>3</sub> nanocolumn bundles	110	10	20.5	23	11	[63]
Plate like NiO/WO <sub>3</sub>	Room temperature	30	4.8	2.5	1.1	[64]
SnO <sub>2</sub> /SnS <sub>2</sub>	80	8	5.3	159	257	[65]
Ag/WO <sub>3</sub> nanofiber	225	5	90.3	_	_	[66]
SnO <sub>2</sub> nanowires	150	2	14	_	_	[67]
ZnO nanowires	150	1	77	37	58	This work
SnO <sub>2</sub> /ZnO nanowires	150	1	45	4	16	This work

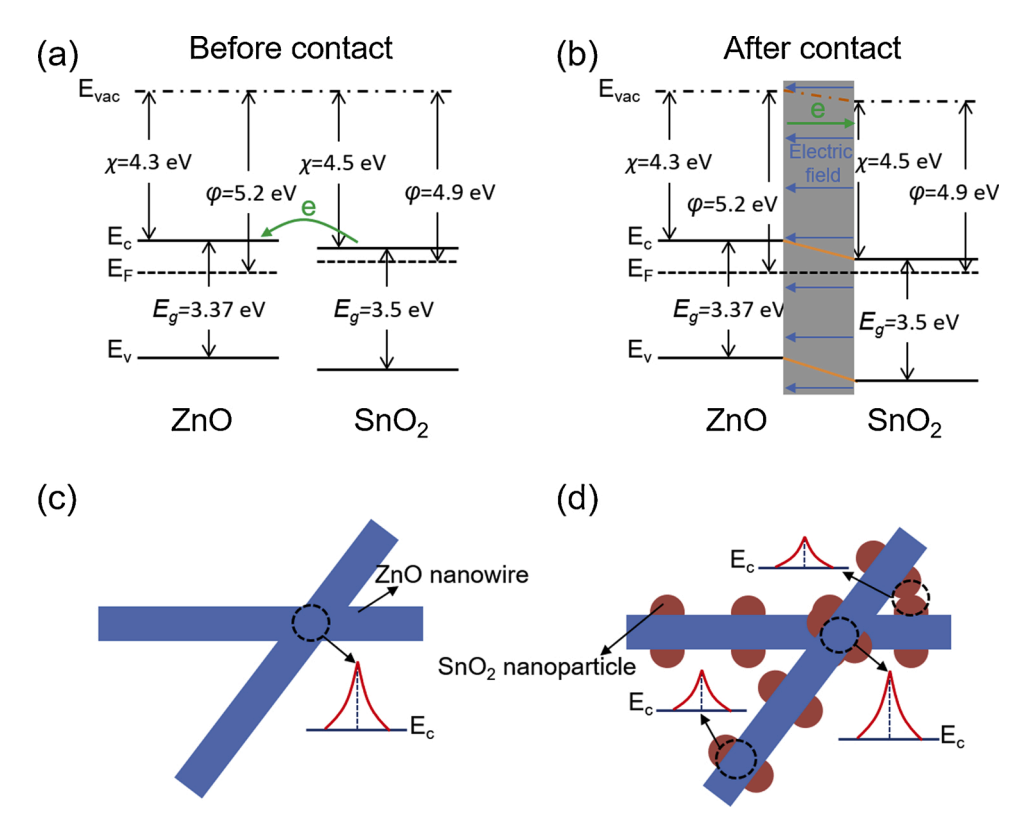


Fig. 10. (a, b) Schematic diagram of the band structure of  $ZnO-SnO_2$  heterostructures. (c, d) Schematic diagram of the potential barriers in pristine ZnO nanowires and  $ZnO-SnO_2$  heterostructures, respectively.

experimental results reported on other hybrid metal oxide composite sensors. For example, Li et al. [77] reported that WO3-SnO2 core-shell structure is more sensitive to reducing gases than oxidizing gas of NO2. On the contrary, Jin et al. [78] found that Ga2O3-ZnO core-shell structure showed a significant improvement in response to oxidizing gas of NO<sub>2</sub> than reducing gases. Therefore, it can be concluded that some other factors besides the depletion model should be considered and involved to understand the sensing mechanism of n-n junctions to oxidizing gases. For the nanowire-based sensors, there are a large number of potential barriers that have to be overcome for the electrons to reach the electrodes. As shown in Fig. 10(c, d), while there is only the potential barrier of ZnO-ZnO in pristine ZnO nanowires network, there are three types of potential barriers for ZnO-SnO<sub>2</sub> heterostructures: (1) the potential barriers at the ZnO-ZnO interfaces of the two adjacent nanowires; (2) the potential barriers at the interfaces between SnO<sub>2</sub>-SnO<sub>2</sub>; (3) the potential barriers at the interfaces of SnO<sub>2</sub> and ZnO. As pointed out previously [79,80], these inter-nanowires potential barriers are modulated by the gas adsorption and desorption, making a great contribution to the gas sensing response. Therefore, the significantly enhanced NO<sub>2</sub> response of Sn/Zn may be more related to the large number of potential barriers built at the interfaces of SnO2-SnO2 and ZnO-SnO2, which are only formed in ZnO-SnO2 heterostructures and are absent in pristine ZnO nanowires.

All in all, because of the extreme complexity of the sensing process, the sensing mechanism of MOS n-n junctions to oxidizing gases has not been well established. In this study, the increased surface free electrons and potential barriers caused by formation of  $\text{ZnO-SnO}_2$  n-n junctions are proposed to be responsible for the highly improved  $\text{NO}_2$  sensing performance of the  $\text{ZnO-SnO}_2$  heterostructures. However, it has to be noted that more in-depth studies are still needed to be carried out to clarify the specific sensing process.

## 4. Conclusion

In summary, ZnO-SnO2 hetero-structured nanowires were successfully prepared via a two-step hydrothermal process. SnO<sub>2</sub> nanoparticles with diameters of 3–5 nm were uniformly grown on the surface of ZnO nanowires to form the ZnO-SnO<sub>2</sub> heterostructures. The diameters of the nanowires are 30-50 nm range and the lengths are in 500 nm to several micrometers range. The NO2 sensing properties of ZnO nanowires were remarkably enhanced by constructing ZnO-SnO2 heterostructure. A strong dependence of NO2 response on the Sn/Zn atomic ratio in the ZnO-SnO<sub>2</sub> heterostructures is observed. Heater temperature of 150 °C was determined as the optimum operating temperature for both pristine ZnO nanowires and ZnO-SnO<sub>2</sub> heterostructures to detect NO<sub>2</sub>, and the Sn/Zn5 sample exhibited the highest NO2 response over the concentration ranging from 250 ppb to 3 ppm. The response of the sensor Sn/ Zn5 to 1 ppm NO<sub>2</sub> was ~45, which was 6.5 times higher than pristine ZnO nanowires. This sensor also exhibited relatively short response/ recovery times of 4/16 s. Notably, the enhancement in response to other interference reducing gases was limited, and thus, the selectivity of ZnO nanowires to NO2 was significantly improved. The enhanced NO2 sensing properties of ZnO-SnO2 heterostructures was mainly ascribed to increased free electrons and potential barriers caused by the ZnO-SnO2 n-n junctions.

## CRediT authorship contribution statement

Sikai Zhao: Conceptualization, Investigation, Writing - original draft. Yanbai Shen: Conceptualization, Resources, Supervision, Writing - review & editing. Roya Maboudian: Conceptualization, Resources, Supervision, Writing - review & editing. Carlo Carraro: Writing - review & editing. Cong Han: Writing - review & editing. Wengang Liu: Writing - review & editing. Dezhou Wei: Supervision.

#### **Declaration of Competing Interest**

The authors declare that they have no known competing financial interests or personal relationships that could have appeared to influence the work reported in this paper.

#### Acknowledgements

The project was supported by the National Natural Science Foundation of China (51674067, 51422402), Fundamental Research Funds for the Central Universities (N180102032, N180106002, N180408018), Liaoning Revitalization Talents Program (XLYC1807160), and Open Foundation of State Environmental Protection Key Laboratory of Mineral Metallurgical Resources Utilization and Pollution Control (HB201902). The research was also supported by the China Scholarship Council (CSC). SZ, CC and RM also acknowledge support of the U.S. National Science Foundation (grant # 1903188). Special thanks are due to the instrument and data analysis from Analytica and Test Center, Northeastern University.

#### Appendix A. Supplementary data

Supplementary material related to this article can be found, in the online version, at doi:https://doi.org/10.1016/j.snb.2021.129613.

#### References

- [1] H. Long, A. Harley-Trochimczyk, T. Pham, Z. Tang, T. Shi, A. Zettl, et al., High surface area MoS2/graphene hybrid aerogel for ultrasensitive NO2 detection, Adv. Funct. Mater. 26 (2016) 5158–5165.
- [2] W. Liu, L. Xu, K. Sheng, C. Chen, X. Zhou, B. Dong, et al., APTES-functionalized thin-walled porous WO3 nanotubes for highly selective sensing of NO2 in a polluted environment, J. Mater. Chem. A 6 (2018) 10976–10989.
- [3] S. Thirumalairajan, K. Girija, V.R. Mastelaro, N. Ponpandian, Surface morphology-dependent room-temperature LaFeO3 nanostructure thin films as selective NO2 gas sensor prepared by radio frequency magnetron sputtering, ACS Appl. Mater. Interfaces 6 (2014) 13917–13927. https://www.epa.gov/no2-pollution.
- [4] D. Buso, M. Post, C. Cantalini, P. Mulvaney, A. Martucci, Gold nanoparticle-doped TiO2 semiconductor thin films: gas sensing properties, Adv. Funct. Mater. 18 (2008) 3843–3849.
- [5] S. Zhao, Y. Shen, X. Yan, P. Zhou, Y. Yin, R. Lu, et al., Complex-surfactant-assisted hydrothermal synthesis of one-dimensional ZnO nanorods for high-performance ethanol gas sensor, Sens. Actuators B Chem. 286 (2019) 501–511.
- [6] X. Chen, Y. Shen, P. Zhou, X. Zhong, G. Li, C. Han, et al., Bimetallic Au/Pd nanoparticles decorated ZnO nanowires for NO2 detection, Sens. Actuators B Chem. 289 (2019) 160–168.
- [7] R. Jaaniso, O.K. Tan, Semiconductor gas sensors (2013).
- [8] N. Yue, J. Weicheng, W. Rongguo, D. Guomin, H. Yifan, Hybrid nanostructures combining graphene–MoS2 quantum dots for gas sensing, J. Mater. Chem. A 4 (2016) 8198–8203.
- [9] T. Li, Y. Shen, S. Zhao, X. Zhong, W. Zhang, C. Han, et al., Sub-ppm level NO2 sensing properties of polyethyleneimine-mediated WO3 nanoparticles synthesized by a one-pot hydrothermal method, J. Alloys. Compd. 783 (2019) 103–112.
- [10] S. Zhao, Y. Shen, P. Zhou, J. Zhang, W. Zhang, X. Chen, et al., Highly selective NO2 sensor based on p-type nanocrystalline NiO thin films prepared by sol–gel dip coating, Ceram. Int. 44 (2018) 753–759.
- [11] S. Zhao, Y. Shen, P. Zhou, X. Zhong, C. Han, Q. Zhao, et al., Design of Au@WO3 core—shell structured nanospheres for ppb-level NO2 sensing, Sens. Actuators B Chem. 282 (2019) 917–926.
- [12] Y. Shen, W. Wang, X. Chen, B. Zhang, D. Wei, S. Gao, et al., Nitrogen dioxide sensing using tungsten oxide microspheres with hierarchical nanorod-assembled architectures by a complexing surfactant-mediated hydrothermal route, J. Mater. Chem. A 4 (2016) 1345–1352.
- [13] Y. Shen, T. Yamazaki, Z. Liu, D. Meng, T. Kikuta, N. Nakatani, Influence of effective surface area on gas sensing properties of WO3 sputtered thin films, Thin Solid Films 517 (2009) 2069–2072.
- [14] J. Xu, Y. Zhang, Y. Chen, Q. Xiang, Q. Pan, L. Shi, Uniform ZnO nanorods can be used to improve the response of ZnO gas sensor, Mater. Sci. Eng. B 150 (2008) 55–60.
- [15] S. Zhao, Y. Shen, P. Zhou, G. Li, C. Han, D. Wei, et al., Influence of synthesis conditions on microstructure and NO2 sensing properties of WO3 porous films synthesized by non-hydrolytic sol–gel method, Nanomaterials 9 (2019) 8.
- [16] P.-P. Zhang, H. Zhang, X.-H. Sun, A uniform porous multilayer-junction thin film for enhanced gas-sensing performance, Nanoscale 8 (2016) 1430–1436.
- [17] X. Zhou, Y. Zhu, W. Luo, Y. Ren, P. Xu, A.A. Elzatahry, et al., Chelation-assisted soft-template synthesis of ordered mesoporous zinc oxides for low concentration gas sensing, J. Mater. Chem. A 4 (2016) 15064–15071.

- [18] Y. Wang, S. Wang, H. Zhang, X. Gao, J. Yang, L. Wang, Brookite TiO2 decorated  $\alpha$ -Fe2O3 nanoheterostructures with rod morphologies for gas sensor application, J. Mater. Chem. A 2 (2014) 7935–7943.
- [19] L. Zhu, Y. Wang, D. Zhang, C. Li, D. Sun, S. Wen, et al., Gas sensors based on metal sulfide Zn1-xCdxS nanowires with excellent performance, ACS Appl. Mater. Interfaces 7 (2015) 20793–20800.
- [20] T. Li, W. Zeng, Z. Wang, Quasi-one-dimensional metal-oxide-based heterostructural gas-sensing materials: a review, Sens. Actuators B Chem. 221 (2015) 1570–1585.
- [21] I.-S. Hwang, E.-B. Lee, S.-J. Kim, J.-K. Choi, J.-H. Cha, H.-J. Lee, et al., Gas sensing properties of SnO2 nanowires on micro-heater, Sens. Actuators B Chem. 154 (2011) 295–300.
- [22] E. Comini, C. Baratto, G. Faglia, M. Ferroni, A. Vomiero, G. Sberveglieri, Quasi-one dimensional metal oxide semiconductors: preparation, characterization and application as chemical sensors, Prog. Mater. Sci. 54 (2009) 1–67.
- [23] X. Chen, Y. Shen, P. Zhou, S. Zhao, X. Zhong, T. Li, et al., NO2 sensing properties of one-pot-synthesized ZnO nanowires with Pd functionalization, Sens. Actuators B Chem. 280 (2019) 151–161.
- [24] Y. Shen, H. Bi, T. Li, X. Zhong, X. Chen, A. Fan, et al., Low-temperature and highly enhanced NO2 sensing performance of Au-functionalized WO3 microspheres with a hierarchical nanostructure, Appl. Surf. Sci. 434 (2018) 922–931.
- [25] T. Li, Y. Shen, S. Zhao, P. Zhou, X. Zhong, S. Gao, et al., Synthesis and in-situ noble metal modification of WO3•0.33H2O nanorods from a tungsten-containing mineral for enhancing NH3 sensing performance, Chinese Chem. Lett. (2020) 2037–2040.
- [26] L. Xu, R. Xing, J. Song, W. Xu, H. Song, ZnO–SnO2 nanotubes surface engineered by Ag nanoparticles: synthesis, characterization, and highly enhanced HCHO gas sensing properties, J. Mater. Chem. C 1 (2013) 2174–2182.
- [27] G. Sberveglieri, Gas Sensors: Principles, Operation and Developments, Springer Science & Business Media, 2012.
- [28] Z. Xue, Z. Cheng, J. Xu, Q. Xiang, X. Wang, J. Xu, Controllable evolution of dual defect Zni and VO associate-rich ZnO nanodishes with (0001) exposed facet and its multiple sensitization effect for ethanol detection, ACS Appl. Mater. Interfaces 9 (2017) 41559–41567.
- [29] Y. Yang, Y. Liang, G. Wang, L. Liu, C. Yuan, T. Yu, et al., Enhanced gas-sensing properties of the hierarchical TiO2 hollow microspheres with exposed high-energy crystal facets, ACS Appl. Mater. Interfaces 7 (2015) 24902–24908.
- [30] N. Singh, A. Ponzoni, R.K. Gupta, P.S. Lee, E. Comini, Synthesis of In2O3–ZnO core-shell nanowires and their application in gas sensing, Sens. Actuators B Chem. 160 (2011) 1346–1351.
- [31] Derek R. Miller, Sheikh A. Akbar, Patricia A. Morris, Nanoscale metal oxide-based heterojunctions for gas sensing: a review, Sens. Actuators B Chem. 204 (2014) 250–272.
- [32] J.M. Walker, S.A. Akbar, Patricia A. Morris, Synergistic effects in gas sensing semiconducting oxide nano-heterostructures: a review, Sens. Actuators B Chem. 286 (2019) 624–640.
- [33] K.J. Choi, H.W. Jang, One-dimensional oxide nanostructures as gas-sensing materials: review and issues, Sensors 10 (2010) 4083–4099.
- [34] K. Wei, S. Zhao, W. Zhang, X. Zhong, T. Li, B. Cui, et al., Controllable synthesis of Zn-doped  $\alpha$ -Fe2O3 nanowires for H2S sensing, Nanomaterials 9 (2019) 994.
- [35] S. Zhao, Y. Shen, P. Zhou, F. Hao, X. Xu, S. Gao, et al., Enhanced NO2 sensing performance of ZnO nanowires functionalized with ultra-fine In2O3 nanoparticles, Sens. Actuators B Chem. (2020), 127729.
- [36] Y. Shen, X. Yan, S. Zhao, X. Chen, D. Wei, S. Gao, et al., Ethanol sensing properties of TeO2 thin films prepared by non-hydrolytic sol–gel process, Sens. Actuators B Chem. 230 (2016) 667–672.
- [37] Y. Liu, D. Xu, T. Cui, H. Yu, X. Li, L. Li, Growth and properties of spinel structure Zn1.8Co0.2TiO4 single crystals by the optical floating zone method, RSC Adv. 9 (2019) 26436–26441.
- [38] J.-M. Themlin, M. Chtaïb, L. Henrard, P. Lambin, J. Darville, J.-M. Gilles, Characterization of tin oxides by x-ray-photoemission spectroscopy, Phys. Rev. B 46 (1992) 2460.
- [39] R. Kim, J.S. Jang, D.H. Kim, J.Y. Kang, H.J. Cho, Y.J. Jeong, et al., A general synthesis of crumpled metal oxide nanosheets as superior chemiresistive sensing layers, Adv. Funct. Mater. 29 (2019), 1903128.
- [40] Y. Huang, G. Li, Q. Fan, M. Zhang, Q. Lan, X. Fan, et al., Facile solution deposition of Cu2ZnSnS4 (CZTS) nano-worm films on FTO substrates and its photoelectrochemical property, Appl. Surf. Sci. 364 (2016) 148–155.
- [41] H. Xia, C. Hong, X. Shi, B. Li, G. Yuan, Q. Yao, et al., Hierarchical heterostructures of Ag nanoparticles decorated MnO2 nanowires as promising electrodes for supercapacitors, J. Mater. Chem. A 3 (2015) 1216–1221.
- [42] H. Yuan, S.A.A.A. Aljneibi, J. Yuan, Y. Wang, H. Liu, J. Fang, et al., ZnO nanosheets abundant in oxygen vacancies derived from metal-organic frameworks for ppblevel gas sensing, Adv. Mater. 31 (2019), 1807161.
- [43] J. Han, Ty. Wang, Tt. Li, H. Yu, Y. Yang, Xt. Dong, Enhanced NOx gas sensing properties of ordered mesoporous WO3/ZnO prepared by electroless plating, Adv. Mater. Interfaces 5 (2018), 1701167.
- [44] O. Lupan, V. Postica, J. Grottrup, A.K. Mishra, N.H. De Leeuw, J.F.C. Carreira, et al., Hybridization of zinc oxide tetrapods for selective gas sensing applications, ACS Appl. Mater. Interfaces 9 (2017) 4084–4099.
- [45] Z. Wang, X. Fan, D. Han, F. Gu, Structural and electronic engineering of 3DOM WO3 by alkali metal doping for improved NO2 sensing performance, Nanoscale 8 (2016) 10622–10631.
- [46] J. Guo, Y. Li, B. Jiang, H. Gao, T. Wang, P. Sun, et al., Xylene gas sensing properties of hydrothermal synthesized SnO2-Co3O4 microstructure, Sens. Actuators B Chem. 310 (2020), 127780.

- [47] Y.-C. Liang, C.-W. Chang, Improvement of ethanol gas-sensing responses of ZnO-WO3 composite nanorods through annealing induced local phase transformation, Nanomaterials 9 (2019) 669.
- [48] M.S. Choi, J.H. Bang, A. Mirzaei, W. Oum, H.G. Na, C. Jin, et al., Promotional effects of ZnO-branching and Au-functionalization on the surface of SnO2 nanowires for NO2 sensing, J. Alloys. Compd. 786 (2019) 27–39.
- [49] A.K. Nayak, R. Ghosh, S. Santra, P.K. Guha, D. Pradhan, Hierarchical nanostructured WO3–SnO2 for selective sensing of volatile organic compounds, Nanoscale 7 (2015) 12460–12473.
- [50] Y.-B. Zhang, J. Yin, L. Li, L.-X. Zhang, L.-J. Bie, Enhanced ethanol gas-sensing properties of flower-like p-CuO/n-ZnO heterojunction nanorods, Sens. Actuators B Chem. 202 (2014) 500-507.
- [51] N.D. Khoang, N. Van Duy, N.D. Hoa, N. Van Hieu, Design of SnO2/ZnO hierarchical nanostructures for enhanced ethanol gas-sensing performance, Sens. Actuators B Chem. 174 (2012) 594–601.
- [52] X. Yang, Q. Yu, S. Zhang, P. Sun, H. Lu, X. Yan, et al., Highly sensitive and selective triethylamine gas sensor based on porous SnO2/Zn2SnO4 composites, Sens. Actuators B Chem. 266 (2018) 213–220.
- [53] M. Wang, Y. Wang, X. Li, C. Ge, S. Hussain, G. Liu, et al., WO3 porous nanosheet arrays with enhanced low temperature NO2 gas sensing performance, Sens. Actuators B Chem. (2020), 128050.
- [54] Z. Zhang, Z. Wen, Z. Ye, L. Zhu, Ultrasensitive ppb-level NO2 gas sensor based on WO3 hollow nanospheres doped with Fe, Appl. Surf. Sci. 434 (2018) 891–897.
- [55] R. Xing, L. Xu, J. Song, C. Zhou, Q. Li, D. Liu, et al., Preparation and gas sensing properties of In2O3/Au nanorods for detection of volatile organic compounds in exhaled breath, Sci. Rep. 5 (2015) 1–14.
- [56] L. Xu, B. Dong, Y. Wang, X. Bai, Q. Liu, H. Song, Electrospinning preparation and room temperature gas sensing properties of porous In2O3 nanotubes and nanowires, Sens. Actuators B Chem. 147 (2010) 531–538.
- [57] L. Gao, Z. Cheng, Q. Xiang, Y. Zhang, J. Xu, Porous corundum-type In2O3 nanosheets: synthesis and NO2 sensing properties, Sens. Actuators B Chem. 208 (2015) 436–443.
- [58] Y. Chen, X. Zhang, Z. Liu, Z. Zeng, H. Zhao, X. Wang, et al., Light enhanced room temperature resistive NO 2 sensor based on a gold-loaded organic-inorganic hybrid perovskite incorporating tin dioxide, Microchim. Ichnoanal. Acta 186 (2019) 47.
- [59] Y. Shen, W. Wang, X. Chen, B. Zhang, D. Wei, S. Gao, et al., Hierarchical nanorod-assembled architectures and nitrogen dioxide sensing of tungsten oxide microspheres by a complexing surfactants-mediated hydrothermal route, J. Mater. Chem. A Mater. Energy Sustain. 4 (2015) 1345–1352.
- [60] J.-H. Cha, S.-J. Choi, S. Yu, I.-D. Kim, 2D WS2-edge functionalized multi-channel carbon nanofibers: effect of WS2 edge-abundant structure on room temperature NO2 sensing, J. Mater. Chem. A 5 (2017) 8725–8732.
- [61] Z. Chen, J. Wang, A. Umar, Y. Wang, H. Li, G. Zhou, Three-dimensional crumpled graphene-based nanosheets with ultrahigh NO2 gas sensibility, ACS Appl. Mater. Interfaces 9 (2017) 11819–11827.
- [62] J.J. Qi, S. Gao, K. Chen, J. Yang, H.W. Zhao, L. Guo, et al., Vertically aligned, double-sided, and self-supported 3D WO3 nanocolumn bundles for lowtemperature gas sensing, J. Mater. Chem. A 3 (2015) 18019–18026.
- [63] M. Bao, Y. Chen, F. Li, J. Ma, T. Lv, Y. Tang, et al., Plate-like p-n heterogeneous NiO/WO3 nanocomposites for high performance room temperature NO2 sensors, Nanoscale 6 (2014) 4063–4066.
- [64] D. Gu, X. Li, Y. Zhao, J. Wang, Enhanced NO2 sensing of SnO2/SnS2 heterojunction based sensor, Sens. Actuators B Chem. 244 (2017) 67–76.
- [65] P. Jaroenapibal, P. Boonma, N. Saksilaporn, M. Horprathum, V. Amornkitbamrung, N. Triroj, Improved NO2 sensing performance of electrospun WO3 nanofibers with silver doping, Sens. Actuators B Chem. 255 (2018) 1831–1840.
- [66] Y.J. Kwon, S.Y. Kang, P. Wu, Y. Peng, S.S. Kim, H.W. Kim, Selective improvement of NO2 gas sensing behavior in SnO2 nanowires by ion-beam irradiation, ACS Appl. Mater. Interfaces 8 (2016) 13646–13658.
- [67] P. Karnati, S. Akbar, P.A. Morris, Conduction mechanisms in one dimensional coreshell nanostructures for gas sensing: a review, Sens. Actuators B Chem. 295 (2019) 127–143.
- [68] W. Xiong, G.M. Kale, Novel high-selectivity NO2 sensor incorporating mixed-oxide electrode, Sens. Actuators B Chem. 114 (2006) 101–108.
- [69] Y. Gönüllü, G.C.M. Rodríguez, B. Saruhan, M. Ürgen, Improvement of gas sensing performance of TiO2 towards NO2 by nano-tubular structuring, Sens. Actuators B Chem. 169 (2012) 151–160.
- [70] D.-X. Ju, H.-Y. Xu, Z.-W. Qiu, Z.-C. Zhang, Q. Xu, J. Zhang, et al., Near room temperature, fast-response, and highly sensitive triethylamine sensor assembled with Au-loaded ZnO/SnO2 core-shell nanorods on flat alumina substrates, ACS Appl. Mater. Interfaces 7 (2015) 19163–19171.

- [71] D.R. Miller, S.A. Akbar, P.A. Morris, Nanoscale metal oxide-based heterojunctions for gas sensing: a review, Sens. Actuators B Chem. 204 (2014) 250–272.
- [72] F. Qu, H. Jiang, M. Yang, Designed formation through a metal organic framework route of ZnO/ZnCo2O4 hollow core-shell nanocages with enhanced gas sensing properties, Nanoscale 8 (2016) 16349–16356.
- [73] X. Zhao, H. Ji, Q. Jia, M. Wang, A nanoscale Co3O4–WO3 p–n junction sensor with enhanced acetone responsivity, J. Mater. Sci. Mater. Electron. 26 (2015) 8217–8223.
- [74] B. Mondal, B. Basumatari, J. Das, C. Roychaudhury, H. Saha, N. Mukherjee, ZnO–SnO2 based composite type gas sensor for selective hydrogen sensing, Sens. Actuators B Chem. 194 (2014) 389–396.
- [75] J.Y. Park, S.-W. Choi, S.S. Kim, A model for the enhancement of gas sensing properties in SnO2–ZnO core–shell nanofibres, J. Phys. D Appl. Phys. 44 (2011), 205403.
- [76] S.W. Choi, A. Katoch, J.H. Kim, S.K. Sang, Prominent reducing gas-sensing performances of n-SnO2 nanowires by local creation of p-n heterojunctions by functionalization with p-Cr2O3 Nanoparticles, ACS Appl. Mater. Interfaces 6 (2014) 17723–17729.
- [77] F. Li, X. Gao, R. Wang, T. Zhang, Design of WO3-SnO2 core-shell nanofibers and their enhanced gas sensing performance based on different work function, Appl. Surf. Sci. 442 (2018) 30–37.
- [78] C. Jin, S. Park, H. Kim, C. Lee, Ultrasensitive multiple networked Ga2O3-core/ZnO-shell nanorod gas sensors, Sens. Actuators B Chem. 161 (2012) 223–228.
- [79] N. Singh, A. Ponzoni, R.K. Gupta, P.S. Lee, E. Comini, Synthesis of In2O3-ZnO coreshell nanowires and their application in gas sensing, Sens. Actuators B Chem. 160 (2011) 1346–1351.
- [80] S. Park, H. Ko, S. Kim, C. Lee, Role of the interfaces in multiple networked onedimensional core-shell nanostructured gas sensors, ACS Appl. Mater. Interfaces 6 (2014), 9595-5600.

**Sikai Zhao** received his M.S. degree from Northeastern University, China, in 2017 and presently is a pH.D. student in the School of Resources and Civil Engineering, Northeastern University, China. His current research interests include gas sensors, low-dimensional and composite nanomaterials.

Yanbai Shen received his pH.D. degree from University of Toyama, Japan, in 2009. He then worked as a researcher at Nagoya University, Japan until 2012. Now, he is a professor in the School of Resources and Civil Engineering, Northeastern University, China. His current research interests include sensors, nanomaterials, oxide semiconductor thin films, intermediate-temperature proton conductors, and fuel cells.

Roya Maboudian is a Professor of chemical engineering at the University of California, Berkeley. She received her pH.D. in applied physics from California Institute of Technology. Her current research interests are in the areas of surface/interfacial science and engineering of micro-/nanosystems, and thin-film science and technology.

Carlo Carraro is a researcher and a lecturer in the Department of Chemical and Biomolecular Engineering at the University of California, Berkeley. He received his bachelor's degree from the University of Padua, Padua, Italy, and his pH.D. degree from California Institute of Technology in Pasadena, California. His research interests are in the physics and chemistry of surfaces and synthesis of novel thin-film materials and processes..

**Cong Han** received his pH.D. degree from Northeastern University, China, in 2013 and presently is a lecturer in School of Resources and Civil Engineering, Northeastern University, China. His current research interests include gas sensors, flotation theory and technology.

**Wengang Liu** is currently a professor in School of Resources and Civil Engineering, Northeastern University, China. His current research interests include gas sensors, mineral processing, flotation theory and technology.

**Dezhou Wei** received his pH.D. degree from Northeastern University, China, in 1990 and presently is a professor in the School of Resources and Civil Engineering, Northeastern University, China. His current research interests include sensors, nanomaterials, microbiological technology of resources and environment, theory, and technology of mineral processing.